Received: 1 October 2020 | Revised: 25 February 2021 | Accepted: 24 March 2021

DOI: 10.1111/jace.17830

Journal of the American Ceramic Society

ORIGINAL ARTICLE

# Properties of irradiated sodium borosilicate glasses from experiment and atomistic simulations

**Mengli Sun**[1,2,3,4] | **Sandro Jahn**[4] | **Haibo Peng**[1] | **Xiaoyang Zhang**[1] | **Tieshan Wang**[1] | **Piotr M. Kowalski**[2,3]

[1]School of Nuclear Science and Technology, Lanzhou University, Lanzhou, China

[2]Institute of Energy and Climate Research (IEK-13), Forschungszentrum Jülich, Jülich, Germany

[3]Jülich Aachen Research Alliance, JARA Energy & Center for Simulation and Data Science (CSD), Jülich, Germany

[4]Institute of Geology and Mineralogy, University of Cologne, Köln, Germany

**Correspondence**
Piotr M. Kowalski, Institute of Energy and Climate Research (IEK-13), Forschungszentrum Jülich, Wilhelm-Johnen-Straße, 52425 Jülich, Germany.
Email: p.kowalski@fz-juelich.de

Tieshan Wang, School of Nuclear Science and Technology, Lanzhou University, Tianshui South Road 222, Lanzhou 730000, China.
Email: tswang@lzu.edu.cn

**Funding information**
Forschungszentrum Jülich; National Natural Science Foundation of China, Grant/Award Number: U1867207; China Scholarship Council; International Atomic Energy Agency, Grant/Award Number: F11022; DSTI Foundation of Gansu, Grant/Award Number: 2018ZX-07

**Abstract**

With a combination of atomistic modeling and experimental techniques, we have investigated the structural and elastic parameters of sodium borosilicate glasses, including irradiation-induced changes. Both approaches show that the Young's modulus depends linearly on the density of material. The simulated glass density and boron speciation match also the estimates by independent, elemental glass composition-based models, indicating that atomistic simulations could be used in validation of theoretical models and experimental results. This allows us to formulate Young's modulus—density relationships for investigated borosilicate glasses and test the existing empirical model for description of Vickers hardness of these materials. The simulation of irradiation reveals a change of $B^{[4]}$ content under irradiation. By applying a simple defects accumulation procedure, we are able to correctly reproduce the measured critical irradiation dose of ~0.1 dpa and provide reasonable information on density change and stored internal energy. With the obtained agreements between the experimental and simulation results, we obtained superior insights into the atomic-scale structural evolution of irradiated borosilicate glasses.

**KEYWORDS**

irradiation effects, MD simulations, mechanical properties, nuclear waste, sodium borosilicate glasses, structure, Young's modulus

## 1 | INTRODUCTION

Borosilicate glasses and melts play an important role in various phenomena, including technological applications or geological processes.[1–5] They are a special kind of silicate glass, mainly made of silica, boron trioxide, and sometimes also other compounds such as sodium oxide and aluminum oxide. They were invented in the early 19th century. Michael Faraday found that boron could be used for making a passable flint glass (a lead borosilicate glass), which was used for the demonstration of magneto-optical *Faraday effect*.[6] The "*heavy glass*" he used in his experiments contained 15.6%

$B_2O_3$ by mass.[6] After detailed systematic studies of the effects of different additions and substitutions to a very common soda lime glass, in the late 19th century, Otto Schott and Ernst Abbe found that a borosilicate glass with significant amount of boron has superior chemical durability and improved thermal shock resistance. For instance, it has three times lower thermal expansion coefficient than the soda lime glass.[6–9] Because of the enhanced performance, borosilicate glasses are technologically applied at extreme conditions, with wide range of applications. These include car headlights, cookwares, such as water bottles, coffee pots or microwave glasses, laboratory apparatus and glassware, and special windows in washing machines or at the international space station.[5,10,11] They are also used as a host of High-Level Nuclear Waste (HLW).[1,3]

In the nuclear applications, the borosilicate glasses are widely used as a primary matrix/host for the immobilization/vitrification of HLW because of good chemical durability and physical parameters, including good thermal stability, resistance to neutral or acid solutions, and the ability to incorporate about 30 different elements or compounds found in spent nuclear fuel.[12,13] They have large waste load (40% HLW by volume) and could be easily formed using low-temperature routes.[1] They are also inexpensive to produce, as boron is abundant worldwide and easily accessible. Besides, the manufacturing technologies are well established.[14,15]

Vitrification has been accepted as one of the most suitable methods to solidify HLW.[1,3,12,14] However, due to safety concerns, it is necessary to estimate the parameters of borosilicate glass under residual irradiation. In the past years, many groups have extensively studied the thermodynamic, chemical and mechanics properties of borosilicate glasses, and significant experimental effort has been devoted to evaluation of the properties of irradiated borosilicate glasses.[16–22] Yet, these experimental results require detailed interpretation, which could be achieved by correct understanding of the atomic-scale processes associated with radiation damage and defects accumulation. It could be achieved with the aid of atomic-scale simulations using supercomputing resources and simulation methods of computational chemistry and materials science.[23,24] In the last decades, different glasses have been investigated at the atomistic scale by atomistic modeling methods, including molecular dynamics. There are various such studies of nuclear glasses that aim to understand the structural and physical–chemical properties of these materials.[1,4,5,7,25–32]

Atomistic modeling methods have been applied to understand the local structure of the glassy materials,[25,30] speciation in glasses or quenched melts,[26] or elastic parameters of such materials.[28,29] At the same time, various techniques were developed to simulate glassy materials and other material compounds under irradiation.[24,26,33,34]

In this contribution we used a combination of experimental measurements and atomistic scale modeling to understand the behavior of irradiated sodium borosilicate glasses and to derive the associated physical parameters. We focus on derivation of the structural, elastic, and thermodynamic properties, such as change in volume, Young's modulus, internal (stored) energy and other parameters that are determined by boron speciation, as well as on understanding the atomic structure of the irradiated glasses and finding structure–property relationships. The reported results also represent a good validation test for the performance of atomistic modeling methods on the simulation of properties of irradiated, structurally complex and disordered materials.

## 2 | METHODS

### 2.1 | Experimental methods

We used the same sample preparation method and multi-energy ion irradiation experiment procedure as Guan et al.[19] The irradiation with multi-energy ions has been applied to obtain uniform damage in the samples, in order to simulate the α-decay-based radiation environment of the vitrified nuclear waste. The irradiation experiment was performed at the Institute of Modern Physics in Lanzhou. The highly energetic Xe ion beams of different energy (1.6, 3.2, and 5 MeV) were induced/selected from an electron cyclotron resonance (ECR) ion source and then redirected to the surfaces of the glass. With ions of multi-energy, uniform damage was created in the sample at room temperature and at the pressure of $7 \times 10^{-5}$ Pa. The penetration range of incident ions was within 2 μm. The used irradiation setup guarantees dominance of nuclear collision processes over electronic effects,[35] which is important for the comparison of the experimental results with the ballistic events-based simulation approach. The dose in displacements per atom (dpa) was derived using standard procedure outlined in detail in our previous studies of irradiation effects on borosilicate glasses.[18]

After irradiation experiments, the nanoindentation measurements were carried out at the Suzhou Institute of Nano-technology and Nano-bionics with the MTS G200 nanoindenter with a three-sided pyramid tip (Berkovich diamond tip). The maximum load on the indenter was ~500 μm and to avoid the influence of glass surface, the indentation at depth larger than 0.3 μm was investigated. These measurements were done in continuous stiffness mode. In Yuan et al.[30] and Guan et al.,[19] we reported the experimental results of the properties of irradiated NBS1 and NBS2 (sodium (Na)-Boron-Silicate) glasses. In addition to those measurements, here we report results of irradiation experiments on one more glass: NBS4[a]. These glass compositions were selected so all three have constant molar ratio of $[SiO_2]/[B_2O_3]$. This allows to

[a]The numbering is not consecutive to preserve the consistency of numeration and naming of the samples measured at Lanzhou University and published in various papers

investigate the influence of the molar ratio of $[Na_2O]/[B_2O_3]$ on the properties of pristine and irradiated borosilicate glasses. The compositions of irradiated glasses are listed in Table 1.

## 2.2 | Computational methods

The atomistic simulations were performed with the aid of force field-based molecular dynamics simulations using the LAMMPS[37] and GULP[38] codes, with the later used to derive the elastic properties of the simulated glass structures. Below we provide detailed description of the applied simulation procedures.

### 2.2.1 | Interaction potentials

A key factor for successful simulation-based studies is the application of a reliable description of interactions between atoms constituting the simulated medium. Because the radiation damage simulations require simulation of a large number of atoms (usually thousands), ab initio simulations are prohibited and classical molecular dynamics with a simple force field has to be applied. In our studies, we used the Buckingham-type interatomic, pair interaction potential of the form:

$$\Phi_{ij} = A_{ij}\exp\left(\frac{-r}{\rho_{ij}}\right) - \frac{C_{ij}}{r^6}, \quad (1)$$

where $r$ is the distance between the interacting atoms and $A_{ij}$, $\rho_{ij}$, and $c_{ij}$ parameters for different pairs of interacting $i$ and $j$ atoms are provided in Table 2. These parameters come from the studies of Guillot and Sator[39] and were fitted to reproduce the thermodynamic, structural and transport properties of natural silicate melts. For the interaction between B and O atoms, we used the force field developed recently and tested on borosilicate glasses by Wang et al.[7] The parameters for the Zn–O interaction were fitted using GULP code,[38] so the interaction potential reproduces the measured structural parameters of ZnO oxide. We note that the used force field parameterization differs from the widely used Kieu et al.[40] scheme, but according to Wang et al.[7] it substantially improves the description of density and boron speciation of borosilicate glasses.

**TABLE 1** Measured (simulated) compositions, and their respective ratios, of borosilicate glasses. The values are in mole percentage. The ratios are defined as follows: $K = [SiO_2]/[B_2O_3]$, $R = ([Na_2O] + [CaO])/[B_2O_3]$, $S - B = [SiO_2]/([SiO_2] + [B_2O_3])$

| Glass ID | $Na_2O$ | $SiO_2$ | $B_2O_3$ | CaO | $TiO_2$ | ZnO | $K$ | $R$ | $S - B$ |
|---|---|---|---|---|---|---|---|---|---|
| G1 glasses | | | | | | | | | |
| 00B[7,36] | 15.2 (15) | 74.8 (75) | 0.0 (0) | 10.1 (10) | | | | | 1.00 (1.00) |
| 06B[7,36] | 16.1 (15) | 69.3 (69) | 4.9 (6) | 9.8 (10) | | | 14.14 (11.50) | 5.29 (4.17) | 0.93 (0.92) |
| 12B[7,36] | 14.8 (15) | 63.8 (63) | 10.8 (12) | 10.6 (10) | | | 5.91 (5.25) | 2.35 (2.08) | 0.86 (0.84) |
| 24B[7,36] | 15.5 (15) | 51.6 (51) | 21.9 (24) | 11.0 (10) | | | 2.36 (2.13) | 1.21 (1.04) | 0.70 (0.68) |
| 37B[7,36] | 14.1 (15) | 36.9 (38) | 38.4 (37) | 10.6 (10) | | | 0.96 (1.03) | 0.64 (0.68) | 0.49 (0.51) |
| 53B[7,36] | 15.0 (15) | 24.9 (25) | 49.3 (50) | 10.8 (10) | | | 0.51 (0.50) | 0.52 (0.50) | 0.34 (0.33) |
| 62B[7,36] | 14.9 (15) | 12.7 (13) | 62.0 (62) | 10.4 (10) | | | 0.20 (0.21) | 0.41 (0.40) | 0.17 (0.17) |
| 75B[7,36] | 15.4 (15) | 0.0 (0) | 74.1 (75) | 10.5 (10) | | | 0.00 (0.00) | 0.35 (0.33) | 0.00 (0.00) |
| PNL 76-68[3,17] | 11.56 (12) | 62.66 (63) | 13.02 (13) | 3.28 (3) | 3.57 (4) | 5.92 (6) | 4.81 (4.85) | 1.14 (1.15) | 0.83 (0.83) |
| G2 glasses | | | | | | | | | |
| SNBS1[32] | 12.0 (12) | 37.7 (38) | 50.3 (50) | | | | 0.75 (0.76) | 0.24 (0.24) | 0.43 (0.43) |
| SNBS2[32] | 12.0 (12) | 44.0 (44) | 44.0 (44) | | | | 1.00 (1.00) | 0.27 (0.27) | 0.50 (0.50) |
| SNBS3[32] | 12.0 (12) | 48.0 (48) | 40.0 (40) | | | | 1.20 (1.20) | 0.30 (0.30) | 0.55 (0.55) |
| SNBS4[32] | 12.0 (12) | 52.8 (53) | 35.2 (35) | | | | 1.50 (1.51) | 0.34 (0.34) | 0.60 (0.60) |
| SNBS5[32] | 12.0 (12) | 58.7 (59) | 29.3 (29) | | | | 2.00 (2.03) | 0.41 (0.41) | 0.67 (0.67) |
| SNBS6[32] | 12.0 (12) | 62.9 (63) | 25.1 (25) | | | | 2.51 (2.52) | 0.48 (0.48) | 0.71 (0.72) |
| SNBS7[32] | 12.0 (12) | 66.0 (66) | 22.0 (22) | | | | 3.00 (3.00) | 0.51 (0.55) | 0.75 (0.75) |
| SNBS8[32] | 12.0 (12) | 68.4 (68) | 19.6 (20) | | | | 3.49 (3.40) | 0.61 (0.60) | 0.78 (0.77) |
| G3 glasses | | | | | | | | | |
| NBS1[20,21,30] | 25.0 (25) | 60.0 (60) | 15.0 (15) | | | | 4.01 (4.00) | 1.67 (1.67) | 0.80 (0.80) |
| NBS2[19,20] | 16.0 (16) | 67.3 (67) | 16.7 (17) | | | | 4.02 (3.94) | 0.96 (0.94) | 0.80 (0.80) |
| NBS4 | 20.0 (20) | 64.0 (64) | 16.0 (16) | | | | 4.00 (4.00) | 1.25 (1.25) | 0.80 (0.80) |

**TABLE 2** Parameters of the interatomic interaction potential (Equation 1)

| Bond | $A_{ij}$ (eV) | $\rho_{ij}$ (Å) | $C_{ij}$ ($eV/Å^6$) |
|---|---|---|---|
| O–O[39] | 9022.79 | 0.265 | 85.0921 |
| Si–O[39] | 50306.10 | 0.161 | 46.2978 |
| B–O[7] | 206941.81 | 0.124 | 35.0018 |
| B–B[7] | 484.40 | 0.350 | 0.0 |
| Si–B[7] | 337.70 | 0.290 | 0.0 |
| Na–O[39] | 120303.80 | 0.170 | 0.0 |
| Ca–O[39] | 155667.70 | 0.178 | 42.2597 |
| Ti–O[39] | 50126.64 | 0.178 | 46.2978 |
| Zn–O[a] | 9791.95 | 0.180 | 0.0 |

[a]Our parameters.

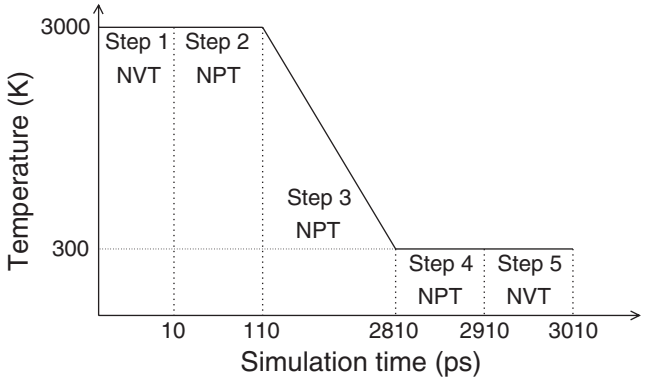


**FIGURE 1** The procedure used to simulate the glass structure. Equivalent of Wang et al.[7]

### 2.2.2 | Simulations of glass structure

In all our simulations, the glasses were represented by models containing ~3000 atoms, with correct number depending on the glass composition (see Table 1 for details). This size of the simulated systems is consistent with the number of atoms used in simulation studies by Wang et al.[7]

The glass structures have been virtually generated following the procedure applied by Wang et al.[7] The procedure is illustrated in Figure 1. We started with a randomly distributed set of atomic positions and such a system has been initially equilibrated for 100 ps at a temperature of 3000 K using NPT (constant pressure–temperature) ensemble. Then, we slowly cooled the system down to 300 K by applying the cooling rate of 1 K/ps. Such simulations ran for 2700 ps. The cooled glasses were further equilibrated for 100 ps at a temperature of 300 K using NPT ensemble. For some alkali metal-rich NBS glasses, we also used NVT (constant volume–temperature) ensemble for cooling, because of problems with obtaining correct glass densities with NPT approach. This procedure follows recommendation of Wang et al.,[7] who noticed that for some glass compositions, NPT ensemble results in uncontrollable expansion in volume. We found that this happens for glasses rich in Na due to formation of a Na-oxide phase, which at high temperatures tends to separate and drastically expand in volume. This could be avoided by lowering the equilibration temperature to below 2000 K. Such a low temperature, however, does not guarantee a well equilibrated structure. The simulations were performed using LAMMPS simulation package.[37]

### 2.2.3 | Simulations of elastic parameters

The elastic Young's modulus as well as bulk ($B$) and shear ($G$) moduli have been simulated on a set of 10 snapshots uniformly selected along the equilibrated trajectory. We used the Voigt–Reuss–Hill approach[41] and the simulations were performed using GULP code.[38] The hardness has been estimated as Vickers hardness, $H_v$, from the following empirical formula derived by Chen et al.[42] for polycrystalline materials and bulk metallic glasses:

$$H_v = 2(k^2G)^{0.585} - 3, \quad (2)$$

In the above equation, $k = G/B$. We notice that it is not intuitive to expect such a simple relationship between hardness, which describes resistance of a material to a localized plastic deformation, and elastic moduli that describe the material's non-permanent elastic resistance to the applied stress. Here we only test if such a simple empirical relationship holds for the measured data on the considered pristine and irradiated borosilicate glasses.

### 2.2.4 | Simulations of accumulation of radiation damage

The radiation damage has been simulated using the defects accumulation procedure applied in previous atomistic simulation studies.[43,44] We performed the damage accumulation molecular dynamics runs in an iterative loop. Each single cation defect formation run was 2 ps long. It consisted of NPT equilibration simulation run (assuming ambient condition), which was followed by a random direction and distance displacement of a randomly selected cation in such a way that the displacement distance was at least 6 Å. This is essential to assure formation of a permanent defect, to which the oxygen sublattice effectively readjusts. Such a simple procedure of gradual defect accumulations has been applied before, for instance, in simulation of radiation damage effects in ceramic materials.[43,45] As a part of our studies, we intended to check if this approach could correctly predict the critical irradiation dose, stored internal energy, or change in Young's modulus

of the measured glasses. We note, however, that in the simulations that are based on simple interaction potentials, we account only for the ballistic effects. Although used experimental setup guarantees dominance of collision events,[35] in reality, electronic structure effects may also impact the response of a material to irradiation. Due to very short simulation times, the simulated dose rate is also orders of magnitude larger than the one realized in experiments[44] and the overall irradiation effects may depend on type and energy of the applied radiation.

#### 2.2.5 | Simulated system

We simulated three different series of borosilicate glasses that reflect the measured compositions of: (G1) Wang et al.,[7] (G2) Zhao et al.,[32] and (G3) Guan et al.[19] The exact compositions are given in Table 1. These could be grouped according to the ratio of alkali to boron ($R = [Na_2O + CaO]/[B_2O_3]$): low (G1 and G2) to high (G1 and G3). In addition, we simulated PNL 76-68 glass discussed by Weber,[17] Manaktala,[3] and Turcotte and Wald.[46]

## 3 | RESULTS

### 3.1 | Pristine glasses

#### 3.1.1 | Physical parameters of the simulated glasses

In order to examine the applicability and reliability of the simple force fields proposed recently by Wang et al.[7] for borosilicate glasses, first we simulated the G1 borosilicate glasses considered by Wang et al.[7] These glasses, in addition to sodium atoms, contain significant amount of calcium ($[Na_2O]/[CaO] = 1.5$). Figures 2 and 3 show the results of such simulations in terms of glass density and boron speciation, respectively. We notice that the simulated density of G1 glass series is slightly, but systematically, higher (by ~3%) than the simulated results of Wang et al.[7] and measurements.[36] However, the experimental trend of density dependence on the boron content is well captured. The density raises with decreasing content of boron, reaching maximum at $[SiO_2]/([SiO_2] + [B_2O_3])$~0.7, and becomes smaller for silicon-rich compositions. Interestingly, our simulations match the results of Wang et al.[7] for silicon-rich glasses, and both simulations overestimate the glass density for these compositions. The offsets between the three datasets could result from slightly different boron speciation in both simulations and experiments. As indicated in Figure 3, in our simulations, there is less $B^{[4]}$ species (by up to 10% of total $B^{[4]}$ content) for boron-rich cases. We carefully

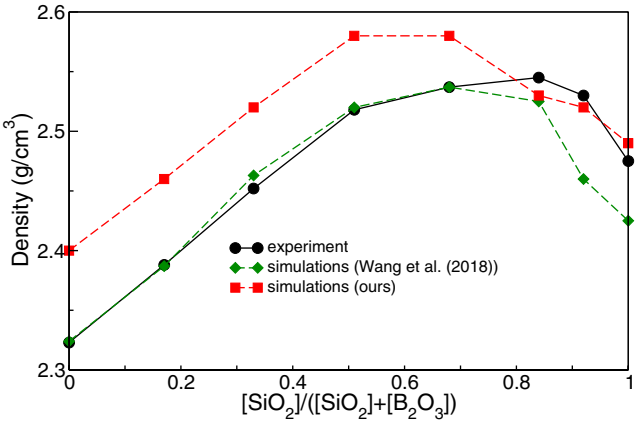


**FIGURE 2** The simulated (red-filled squares) and measured (black-filled circles[7,36,47]) density of G1 glasses. In addition, densities simulated by Wang et al.[7] are shown [Color figure can be viewed at wileyonlinelibrary.com]

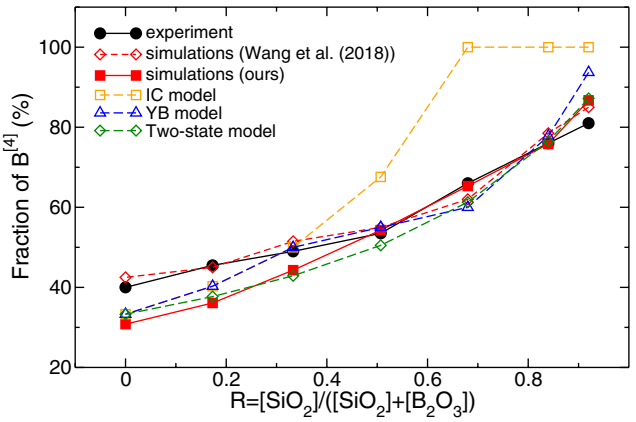


**FIGURE 3** The fraction of $B^{[4]}$ in G1 glasses. The points represent: measured values (black-filled circles[36]), our simulations (red-filled squares), simulations of Ref. 7 (red diamonds), IC model (orange squares[36]), YB model (blue triangles[48]) and two-state model (green diamonds[36]). IC, ideal counting; YB, Yun–Bray [Color figure can be viewed at wileyonlinelibrary.com]

discuss this discrepancy with the aid of the existing theoretical models.

The formation of $B^{[4]}$ species occurs through the presence of alkaline metals, Ca, and Na atoms in our case. These atoms act as charge-compensating network modifiers.[36] Thus, one should expect that the number of $B^{[4]}$ species will be limited by the amount of available alkali elements. For the case without silicon, we could estimate this limit as:

$$[B^{[4]}] \sim \frac{2[Na_2O] + 2[CaO]}{2[B_2O_3]}. \quad (3)$$

For the G1 75B glass, this results in $B^{[4]}$ content of 0.3333. The value of 0.4 reported by Wang et al.[7] exceeds this limit (Figure 3).

On the other hand, our value of 0.31 is well consistent with the provided estimate. In Table 1, we provide the estimate obtained with Equation (3). It well describes the simulated values for the cases when $[B_2O_3] > [SiO_4]$ (and $[B_2O_3] < [Na_2O + CaO]$), but overestimates the amount of $B^{[4]}$ for Si-rich compositions. This is understandable as fraction of the alkali metals should participate in saturation of Si–O chains.[36]

According to Smedskjaer et al.,[36] there exist three models that describe the $B^{[4]}$ content as a function of composition in a borosilicate glass, similarly to Equation (3). The ideal counting (IC) model[36] assumes the equal charge-compensating effect of modifiers (Na and $Ca^{2+}$ ions) on $B^{[4]}$ speciation, and $B^{[4]}$ occurs in corner-sharing pairs that are fully bounded (connected) to $B^{[3]}$ or $SiO_4$ tetrahedra units. In that model, the excess of alkali atoms create non-bridging oxygen (NBO) on these $B^{[3]}$ or $SiO_4$ units. As discussed by Smedskjaer et al.,[36] this model creates too many $B^{[4]}$ units for G1 glass with low concentration of B when $[B_2O_3] < [Na_2O + CaO]$. The Yun–Bray (YB) model[48] assumes that at higher concentration of modifiers, the add-atoms modify $SiO_4$ tetrahedra by the formation of NBO only on $SiO_4$ tetrahedra units, while $BO_3$ units are less affected. It produces improved description of the $B^{[4]}$ content but still overestimates the amount of $B^{[4]}$ in G1 glasses at high Si content. Both models predict experimentally unseen saturation (as limit of $B^{[4]} = 1$ has not been reached experimentally). The experimental results indicate competition between the formation of $B^{[4]}$ species and NBO for high Si content/low B content.[36] It is accounted for in a two-state model of Smedskjaer et al.,[36] where the enthalpy difference ($\Delta H$) between the formation of $B^{[4]}$ species and NBO on $SiO_4$ is taken into account. The results of all three models for G1 glasses are reported in Table 3 and Figure 3, which are equivalent to Figure 6 of Smedskjaer et al.[36] Interestingly, the simulated data could be well fitted with the two-state model assuming $\Delta H = 0.072$ eV (as proposed by Smedskjaer et al.[36]). The fact that all the models reproduce well the simulated data at low alkali content validates our simulations and points toward potential overestimation of $B^{[4]}$ content in data of Smedskjaer et al.,[36] as also indicated in Figure 6 of Smedskjaer et al.[36]

In the next step, we performed simulations of the series of SNBS G2 glasses investigated by Zhao et al.[32] Zhao et al.[32] measured and simulated (with the similar force field-based

**TABLE 3** Model-predicted, simulated, and experimental fraction of $B^{[4]}$ and density (in g/cm$^3$) of G1–G3 glasses

| Glass | $\rho_{exp}$ | $\rho_{sim}$ | $\rho_{FF}$ | $\rho_{BF}$ | $\rho_{In}$ | $\rho^{In}_{sim}$ | $B^{[4]}_{exp}$ | $B^{[4]}_{sim}$ | $B^{[4]}_{IC}$ | $B^{[4]}_{YB}$ | $B^{[4]}_{Two\text{ - }state}$ | $B^{[4]In}_{sim}$ |
|---|---|---|---|---|---|---|---|---|---|---|---|---|
| G1 glass | | | | | | | | | | | | |
| 00B[7,36] | 2.48 | 2.49 | — | — | — | — | — | — | — | — | — | — |
| 06B[7,36] | 2.53 | 2.52 | 2.52 | 2.61 | 2.48 | — | 0.81 | 0.87 | 1.00 | 0.94 | 0.87 | — |
| 12B[7,36] | 2.55 | 2.53 | 2.51 | 2.56 | 2.49 | — | 0.76 | 0.76 | 1.00 | 0.78 | 0.76 | — |
| 24B[7,36] | 2.54 | 2.58 | 2.46 | 2.47 | 2.47 | — | 0.66 | 0.65 | 1.00 | 0.60 | 0.61 | — |
| 37B[7,36] | 2.52 | 2.58 | 2.41 | 2.38 | 2.45 | — | 0.54 | 0.54 | 0.68 | 0.55 | 0.51 | — |
| 53B[7,36] | 2.45 | 2.52 | 2.35 | 2.31 | 2.40 | — | 0.49 | 0.44 | 0.50 | 0.50 | 0.43 | — |
| 62B[7,36] | 2.39 | 2.46 | 2.26 | 2.24 | 2.41 | — | 0.46 | 0.36 | 0.40 | 0.40 | 0.38 | — |
| 75B[7,36] | 2.32 | 2.40 | 2.18 | 2.18 | — | — | 0.40 | 0.31 | 0.33 | 0.33 | 0.33 | — |
| G2 glass | | | | | | | | | | | | |
| SNBS1[32] | 2.16 | 2.40 | 2.32 | 2.12 | 2.42 | — | — | 0.24 | 0.24 | 0.24 | 0.22 | — |
| SNBS2[32] | 2.16 | 2.42 | 2.34 | 2.15 | 2.43 | — | — | 0.27 | 0.27 | 0.27 | 0.25 | — |
| SNBS3[32] | 2.18 | 2.44 | 2.35 | 2.17 | 2.43 | — | — | 0.28 | 0.30 | 0.30 | 0.26 | — |
| SNBS4[32] | 2.24 | 2.45 | 2.37 | 2.19 | 2.43 | — | — | 0.31 | 0.34 | 0.34 | 0.29 | — |
| SNBS5[32] | 2.25 | 2.46 | 2.33 | 2.23 | 2.36 | — | — | 0.35 | 0.41 | 0.41 | 0.34 | — |
| SNBS6[32] | 2.32 | 2.45 | 2.36 | 2.25 | 2.39 | — | — | 0.40 | 0.48 | 0.48 | 0.37 | — |
| SNBS7[32] | 2.34 | 2.46 | 2.38 | 2.26 | 2.40 | — | — | 0.42 | 0.55 | 0.55 | 0.41 | — |
| SNBS8[32] | 2.35 | 2.48 | 2.40 | 2.27 | 2.42 | — | — | 0.43 | 0.60 | 0.60 | 0.44 | — |
| G3 glass | | | | | | | | | | | | |
| NBS1[20,21,30] | 2.36 | 2.37 | 2.49 | 2.52 | 2.53 | 2.57 | 0.77 | 0.64 | 1.00 | 0.70 | 0.89 | 0.82 |
| NBS2[19,20] | 2.28 | 2.37 | 2.45 | 2.36 | 2.48 | 2.56 | 0.70 | 0.53 | 0.94 | 0.74 | 0.51 | 0.65 |
| NBS4 | 2.50 | 2.42 | 2.47 | 2.43 | 2.51 | 2.56 | — | 0.64 | 1.00 | 0.73 | 0.67 | 0.74 |

The supscripts/superscripts indicate: exp (experiment), sim (simulations), FF (model od Feil and Feller[50], BF (model of Budhwani and Feller51), In (model of Inoue et al.[52]), IC (Ideal counting model[36]), YB (Yun–Bray model[48]) and Two-state (model of of Smedskjaer et al.[36])

method) the Young's modulus and hardness of these materials. However, in these simulation studies, the potential of Kieu et al.[40] was used, which according to Wang et al.[7] cannot correctly capture the density and boron speciation of borosilicate glass. The results of simulations of density and boron speciation with the Wang et al.[7] potential are reported in Figures 4 and 5. Our simulations predict a density of ~2.40 – 2.47 g/cm$^3$ for this class of glasses. This is by 10% larger than the experimental densities reported by Zhao et al.[32] However, our result is very close to other experimental and simulation studies by Barlet et al.[49] of glass of similar composition, and in general within a density range expected for borosilicate glasses.[49] In order to shed light on this discrepancy, we applied the models of glass densities as a function of composition analyzed by Barlet et al.[49]: (M1) Feil and Feller,[50] (M2) Budhwani and Feller[51] and (M3) Inoue et al.[52] as the most accurate model. The results are reported in Table 3 and in Figure 4. We note that the simulated densities are consistent with the model of Inoue et al.[52] On the other hand, model of Budhwani and Feller[51] is consistent with the measured densities, but as discussed by Barlet et al.,[49] it, in general, underestimates the densities. With these results, we thus suspect that the experimental densities reported by Zhao et al.[32] are somehow underestimated or that the real parameters of the investigated glasses were slightly different.

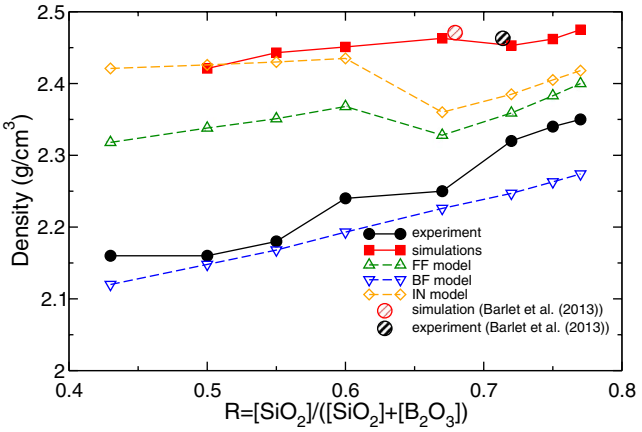


**FIGURE 4** Density of G2 glasses. The symbols represent the results of: our simulations (red squares), experimental results (black circles[32]; semi-filled circles[49]), model M1 (FF, green up-triangles[50]), model M2 (BF, blue down triangles[51]), and model M3 (orange diamonds[52]) [Color figure can be viewed at wileyonlinelibrary.com]

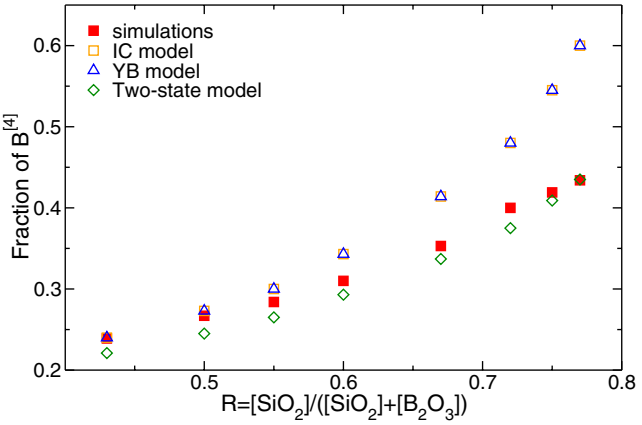


**FIGURE 5** Content of B$^{[4]}$ in G2 glasses. The points represent the results of our simulations (filled red squares), the ideal counting model (IC, orange squares[36]), the Yun–Bray model (YB, blue triangles[48]), and the two-state model (green diamonds[36]) [Color figure can be viewed at wileyonlinelibrary.com]

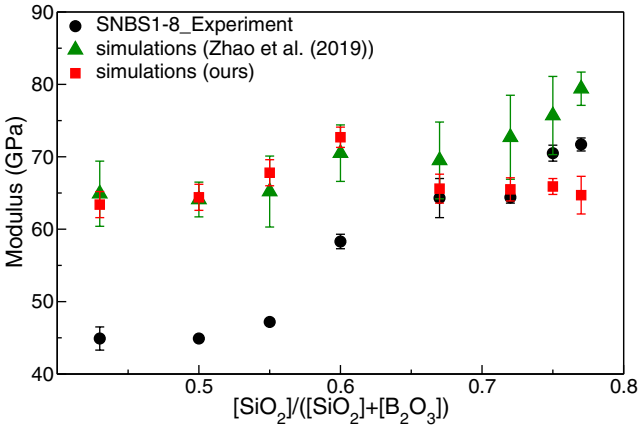


**FIGURE 6** Young's modulus of G2 glasses. The points represent the measured values (black-filled circles[32]), our simulations (red-filled squares), and simulations of Ref. 32 (filled green triangles) [Color figure can be viewed at wileyonlinelibrary.com]

The predictions of the models for the fraction of B$^{[4]}$ and density, together with the experimental data are reported in Table 3.

The results obtained for the two series of glasses (G1 and G2) indicate that the applied simulation procedure results in production of glass structures with reasonable density and boron speciation, which is important in terms of analysis of the elastic properties of glasses and their performance under irradiation.

### 3.1.2 | Elastic properties

The simulated and measured Young's modulus for the series of G2 SNBS glasses of Zhao et al.[32] are reported in Figure 6. The simulations show the Young's modulus of ~65–70 GPa, with no clear dependence on the glass composition (B content). This is in contradiction to the experimental results, which show much lower modulus for B-rich compositions (~45 GPa), but similar for Si-rich glasses, ~70 GPa. Interestingly, for Si-rich compositions, we observe the best agreement between the measured and simulated densities (Figure 4), and our simulated values are well consistent with the simulation results of Zhao et al.[32] In Figure 7, we show

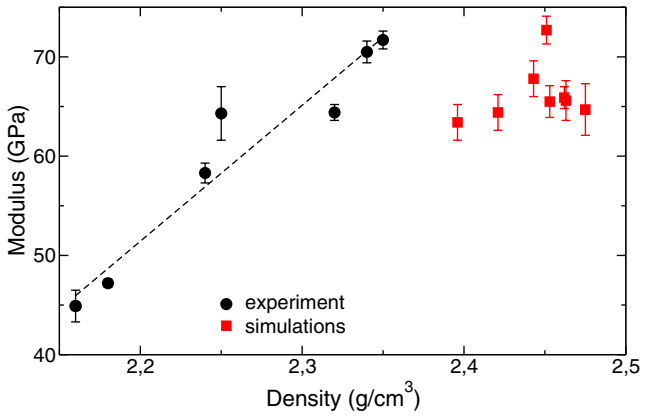


**FIGURE 7** Young's modulus as a function of density for G2 glasses. The points represent the experimental results (filled black circles[32]) and our simulations (filled red squares) [Color figure can be viewed at wileyonlinelibrary.com]

the Young's modulus dependence on glass density. The experimental measurements show a clear, linear-like trend with Young's modulus ($E$) well approximated by:

$$E(\text{GPa}) \sim 125\rho - 224. \quad (4)$$

where $\rho$ is the density given in g/cm$^3$. The simulated data show much less variation with density, because of nearly identical densities (Figure 6; Table 3). The difference between the simulated and measured Young's modulus must reflect the differences in the measured and simulated glass structures, namely $B^{[4]}$ speciation. The simulated boron speciation is given in Figure 5 and Table 3, and it is well consistent with the models discussed in Section 3.1.1.

The hardness of G2 SNBS glasses estimated as Vickers hardness from the computed bulk and shear moduli is provided in Table 4. We note that Zhao et al.[32] performed direct molecular dynamics simulations of hardness of these glasses and obtained values that are one order of magnitude larger than the measured values. Both datasets are provided in Table 4. On the other hand, our estimate matches reasonably well the measured values. This indicates that a simple, empirical relationship between hardness and elastic moduli derived by Chen et al.[42] for polycrystalline materials and bulk metallic glasses can be successfully applied to estimate the hardness of glassy materials. On the other hand, our analysis indicates some problems with the data on hardness simulated explicitly by Zhao et al.[32] We note, however, that such direct simulations as performed by Zhao et al.[32] are not trivial and several factors can impact the quality of the simulated values.

## 3.2 | Irradiated glasses

Here we intended to perform simulations of irradiation of series of G3 glasses, in order to interpret experimental data published recently [19,20,21,30] and produced within the scope of this paper (NBS4 glass). The computational procedure is tested on data on irradiated PNL 76-68 glass.[17,46] The presented comparison between the experimental and simulation results should be considered having in mind all the limitations of the simulation method and difference in simulated conditions from those realized in experimental irradiation studies, as mentioned in Section 2.2.4.

### 3.2.1 | Properties of PNL 76-68 glass

In order to validate the simulation procedure for simulation of irradiated glasses, we simulated the PNL 76-68 glass for which the irradiation-induced (stored) internal energy and volume change have been experimentally measured.[17,46] We selected this glass composition as this is the least compositionally complex of the measured glasses and the required potential parameters are known for all the elements, except for Zn (which we fitted here). However, this glass is a good test case because experimentally it shows uniquely negligible volume (density) change and significant stored internal energy (of ~90 J/g; Figure 8). We thus tested how our computational setup reproduces these data. The results are given in Figure 8. Indeed, our simulation shows negligible volume/density change (within 1%) and the simulated stored energy of ~80 J/g is also very consistent with the experimental value,

**TABLE 4** The parameters of the pristine G2 glasses obtained from the experiment (exp)[32] and simulations (sim): ours and Zhao et al.[32] (marked with[a]). The units are GPa

| Glass | $E_{exp}$ | $E_{sim}$ | $E^a_{sim}$ | $H_{exp}$ | $H_{sim}$ | $H^a_{sim}$ |
|---|---|---|---|---|---|---|
| SNBS1 | 44.9 ± 1.6 | 63.4 ± 1.8 | 64.9 ± 4.5 | 3.9 ± 0.2 | 3.5 ± 0.7 | 19.6 ± 1.6 |
| SNBS2 | 44.9 ± 0.4 | 64.4 ± 1.8 | 64.1 ± 2.4 | 4.2 ± 0.1 | 3.4 ± 0.3 | 22.5 ± 1.9 |
| SNBS3 | 47.2 ± 0.4 | 67.8 ± 1.8 | 65.2 ± 4.9 | 4.4 ± 0.1 | 4.5 ± 0.3 | 22.3 ± 3.2 |
| SNBS4 | 58.3 ± 1.0 | 72.7 ± 1.4 | 70.5 ± 3.9 | 5.6 ± 0.2 | 5.0 ± 1.2 | 23.9 ± 2.8 |
| SNBS5 | 64.3 ± 2.7 | 65.6 ± 2.0 | 69.5 ± 5.3 | 6.1 ± 0.3 | 5.0 ± 0.5 | 25.2 ± 3.0 |
| SNBS6 | 64.4 ± 0.8 | 65.5 ± 1.6 | 72.7 ± 5.8 | 6.1 ± 0.2 | 4.8 ± 0.4 | 24.8 ± 2.1 |
| SNBS7 | 70.5 ± 1.1 | 65.9 ± 1.1 | 75.7 ± 5.4 | 6.6 ± 0.1 | 5.6 ± 0.3 | 26.4 ± 1.9 |
| SNBS8 | 71.7 ± 0.9 | 64.7 ± 2.6 | 79.4 ± 2.3 | 6.5 ± 0.2 | 5.3 ± 0.5 | 27.5 ± 1.9 |

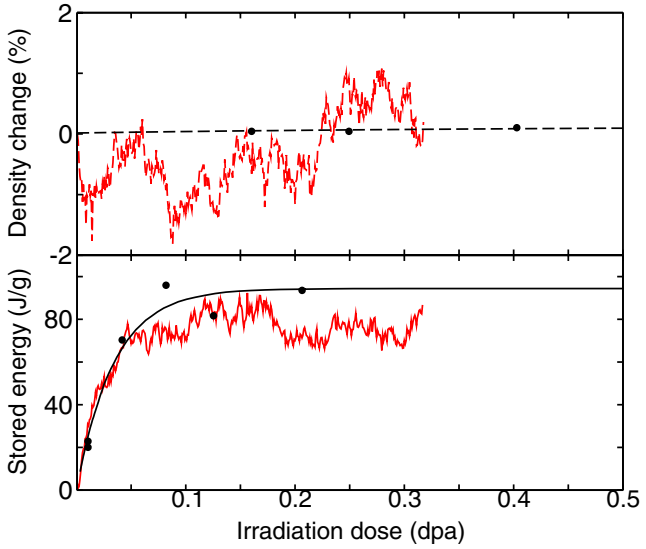


**FIGURE 8** The simulated (red line) and measured (filled black circles[17,54]) density and internal stored energy of irradiated PNL 76-68 glass. The experimental irradiation fluence was rescaled to match the simulated change in the stored internal energy (at low irradiation dose <0.05 dpa) [Color figure can be viewed at wileyonlinelibrary.com]

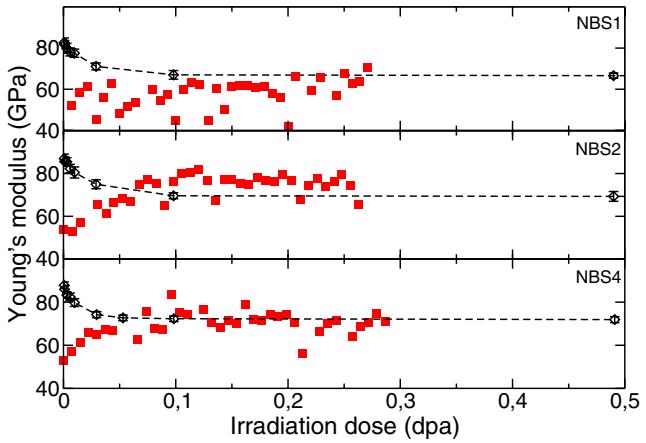


**FIGURE 9** The simulated (filled red squares) and measured (black diamonds[19] and our studies) Young's modulus for series of irradiated G3 glasses [Color figure can be viewed at wileyonlinelibrary.com]

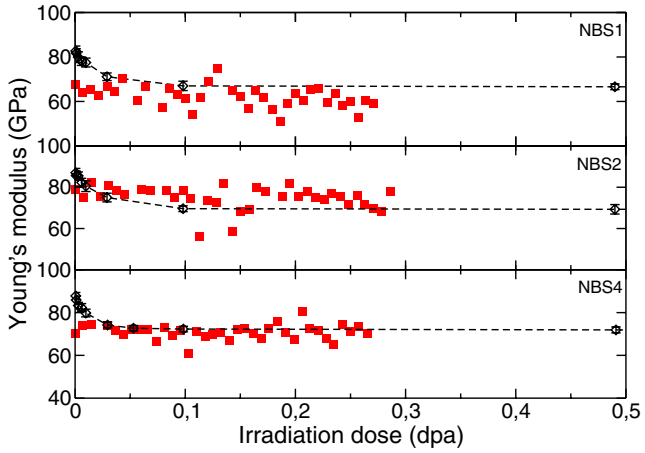


**FIGURE 10** The simulated (filled red squares) and measured (black diamonds[19] and our studies) Young's modulus for series of irradiated G3 glasses obtained from simulation assuming pristine glass density as provided by the model of Inoue et al.[52] [Color figure can be viewed at wileyonlinelibrary.com]

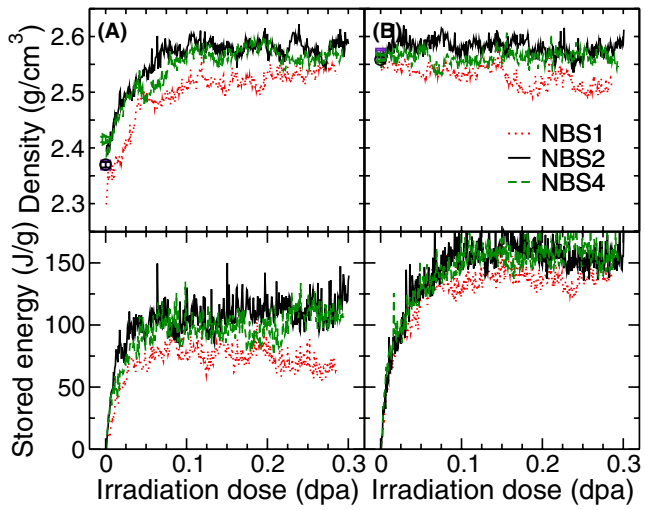


**FIGURE 11** The simulated density and internal stored energy for series of G3 glasses, obtained from simulation assuming pristine glass density as (A) simulated here with NPT cooling procedure and (B) with NVT cooling procedure assuming glass density/volume predicted by the model of Inoue et al.[52] NPT, constant pressure–temperature; NVT, constant volume–temperature [Color figure can be viewed at wileyonlinelibrary.com]

considering simplistic description of the interatomic interactions and irradiation effects. We are thus confident that with the applied simulation procedure, the irradiation effects could be effectively simulated.

### 3.2.2 | Properties of G3 glasses: Experimental data

Guan et al.[19] and Peng et al.[20] measured change in volume and Young's modulus for the irradiated G3 NBS1 and NBS2 glasses. The results on Young's modulus are given in Figure 9. Interestingly, the data show saturated accumulation of radiation damage at critical irradiation dose of ~0.1 dpa. In Figure 9, we also present the experimental data for one more glass compositions (NBS4). All of the considered compositions have similar $K$ parameter, which allows for investigation of the impact of silicon content on the property of the irradiated glass. Regarding the elastic and mechanical properties, on the experimental side, the irradiation causes the decrease in the Young's modulus and hardness. For instance,

the Young's modulus of NBS2 glass decreases from 85 GPa (unirradiated case) to 70 GPa. In view of our analysis of behavior of borosilicate glasses provided in previous sections, this indicates decrease in glass density and $B^{[4]}$ content. In order to understand these effects, we performed molecular dynamics simulation of irradiation process.

### 3.2.3 | Properties of G3 glasses: Simulations

The simulated properties of irradiated G3 NBS1, NBS2 and NBS4 glasses are reported in Figures 9–12 and Tables 5 and 6. First, we report the simulated change in Young's modulus.

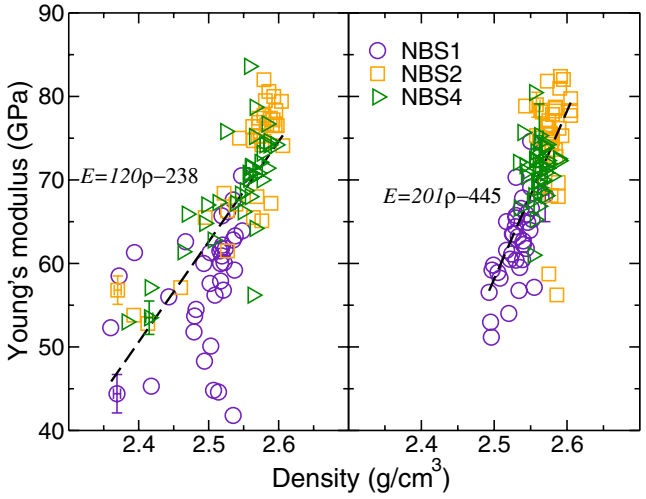


**FIGURE 12** The simulated Young's modulus for series of irradiated G3 glasses. The two panels show the results with NPT (left panel) and NVT (right panel) ensembles (see text for detailed explanation). The dashed lines represent linear fits to the data. NPT, constant pressure–temperature; NVT, constant volume–temperature [Color figure can be viewed at wileyonlinelibrary.com]

Interestingly, the Young's modulus of the pristine glasses is substantially smaller than the measured value (~50 GPa vs. ~90 GPa), and the simulations show increase in the modulus during irradiation (Figure 9). On the other hand, experiments and simulations give consistent value of ~70 GPa for irradiated glass after the critical dose of 0.1 dpa. The difference seen between the experimental and simulated cases could be explained by the difference in measured and computed glass density and boron speciation. As indicated in Figure 11a, the density of the "virtually" irradiated glasses increases by ~10%. As a result, the simulated Young's modulus increases by ~50%, from ~50 to 75 GPa. This is consistent with the model (Equation 4). The increase in density is accompanied by increase in the $B^{[4]}$ content (see Table 5). The increase in the Young's modulus in simulated irradiated glass is thus clearly correlated with the increase in $B^{[4]}$ content of the irradiated glass.

However, we noticed that the simulated densities of G3 glasses are inconsistent with the best theoretical prediction ($\rho_{in}$ in Table 3), and the simulated glasses have substantially lower densities. The discrepancy is more pronounced for the glass compositions with large sodium content. In fact, we noticed some convergence problems with simulations of NBS1 glass (highest sodium content) and suspect that high abundance of sodium affects the simulated cooling procedure (see Section 2.2.2). This results in not well equilibrated final glass structures. In order to correct for the density effect, we thus performed the simulations by applying NVT ensemble for cooling (glass preparation), assuming glass density provided by the model of Inoue et al.[52] The results with so "virtually" prepared glass are provided in Figures 10 and 11b, and Table 6. Now, we get much better agreement with the experiment regarding Young's modulus of pristine glasses. The simulated properties of irradiated glasses, however, are not that sensitive to the simulation setup (Figures 9–12).

**TABLE 5** The parameters of the pristine (p) and irradiated (i) G3 glasses obtained from simulation (sim) and experiment (exp). The units are g/cm$^3$ (density $\rho$) and GPa ($E$ and $H$)

| Glass | $\rho_p$ | $E_p$ | $E_p^{exp}$ | $H_p$ | $H_p^{exp}$ | $B_p^{[4]}$ | $\rho_i$ | $E_i$ | $E_i^{exp}$ | $H_i$ | $H_i^{exp}$ | $B_i^{[4]}$ |
|---|---|---|---|---|---|---|---|---|---|---|---|---|
| NBS1[20,21,30] | 2.37 | 44.4 | 82.7 ± 2.2 | 3.8 | 7.0 ± 0.3 | 0.64 | 2.53 | 62.7 | 66.6 ± 1.3 | 3.9 | 4.3 ± 0.2 | 0.73 |
| NBS2[19,20] | 2.37 | 56.8 | 87.0 ± 2.1 | 5.2 | 7.6 ± 0.3 | 0.53 | 2.59 | 80.7 | 69.3 ± 2.3 | 6.3 | 4.6 ± 0.2 | 0.55 |
| NBS4 | 2.42 | 53.5 | 87.8 ± 1.6 | 5.0 | 7.7 ± 0.3 | 0.64 | 2.56 | 70.8 | 71.9 ± 1.4 | 4.8 | 4.9 ± 0.2 | 0.64 |

**TABLE 6** The parameters of the pristine (p) and irradiated (i) G3 glasses obtained from simulation (sim) assuming pristine glass density as provided by model of Inoue et al.[52] and experiment (exp). The units are g/cm$^3$ (density $\rho$) and GPa ($E$ and $H$)

| Glass | $\rho_p$ | $E_p$ | $E_p^{exp}$ | $H_p$ | $H_p^{exp}$ | $B_p^{[4]}$ | $\rho_i$ | $E_i$ | $E_i^{exp}$ | $H_i$ | $H_i^{exp}$ | $B_i^{[4]}$ |
|---|---|---|---|---|---|---|---|---|---|---|---|---|
| NBS1[20,21,30] | 2.57 | 68.2 | 82.7 ± 2.2 | 5.3 | 7.0 ± 0.3 | 0.82 | 2.51 | 58.6 | 66.6 ± 1.3 | 3.7 | 4.3 ± 0.2 | 0.71 |
| NBS2[19,20] | 2.56 | 79.0 | 87.0 ± 2.1 | 6.5 | 7.6 ± 0.3 | 0.65 | 2.61 | 73.9 | 69.3 ± 2.3 | 4.5 | 4.6 ± 0.2 | 0.57 |
| NBS4 | 2.56 | 75.3 | 87.8 ± 1.6 | 5.4 | 7.7 ± 0.3 | 0.74 | 2.55 | 69.1 | 71.9 ± 1.4 | 4.4 | 4.9 ± 0.2 | 0.75 |

In Figure 12, we provide information on dependence of the Young's modulus on the glass density during the irradiation simulation runs. We observe strong correlations that resemble these seen experimentally (Figure 6 and Equation 4). Both experiment and simulation thus show linear-like increase of Young's modulus with increase of density. The Vickers hardness estimated from the simulated elastic moduli is also well consistent with the measured values (Tables 5 and 6).

In Figure 11, we present the simulated stored internal energy of G3 glasses. We notice that, although the two applied glass preparation schemes result in slightly different densities and structure of pristine glasses (Tables 5 and 6) and thus resulting stored internal energy, the density of irradiated glasses and critical irradiation doses are nearly identical. The obtained values are also qualitatively consistent with the experimental and simulated results for PNL 76-68 glass (Figure 8).

## 4 | CONCLUSIONS

We performed extensive simulations and experimental measurements of the structural and elastic parameters of series of borosilicate nuclear glasses under irradiation. With the larger composition-dependent set of simulated and measured glass parameters, we performed in depth analysis of the structure–property relationships in these materials, focusing on glass density, boron speciation, elastic Young's modulus and hardness. We found that the properties of borosilicate glasses are mainly determined by the glass elemental composition and the density. The simulated glass density follows well the prediction of the model by Inoue et al.,[52] and the boron speciation, namely the content of $B^{[4]}$, is well described by the two-state model of Smedskjaer et al.[36] We found a clear linear relationship between density and Young's modulus. The hardness of the measured glasses is also reasonably well estimated from the knowledge of the bulk and shear moduli by a simple empirical relationship proposed by Chen et al.[42] This is an interesting result, as it is rather "non-intuitive" that hardness could be estimated from parameters that describe only the resistance of a material to elastic deformations.

The simulations of glasses under irradiation show that a simple defect accumulation procedure can capture well the irradiation process, correctly predicting the critical irradiation dose (~0.1 dpa), change in density and elastic/mechanical properties, and give reasonable estimate for the stored internal energy. The simulations results and the existing models for glass density and $B^{[4]}$ content indicate potential problems with characterization of the measured samples. This shows the power and importance of atomistic simulations of glassy materials for correct interpretation of the experimental data.

## ACKNOWLEDGMENTS

MS thanks CSC-China Scholarship Council for funding her PhD studies research at Forschungszentrum Jülich (IEK-6 and IEK-13 Institutes)/University of Cologne in Germany. We thank the JARA-HPC awarding body for time on the RWTH University and Forschungszentrum Jülich supercomputing resources awarded through JARA-HPC Partition. SJ and MS gratefully acknowledge the Gauss Centre for Supercomputing e.V. for providing computing time (project ID CHPO15) through the John von Neumann Institute for Computing (NIC) on the JUWELS supercomputer at Jülich Supercomputing Centre (JSC). HP thanks for support by INWARD coordinated research project (Ion Beam Irradiation for High-Level Nuclear Waste Form Development, F11022) from IAEA. The authors thank the National Natural Science Foundation of China (grant no. U1867207), and DSTI Foundation of Gansu (grant no. 2018ZX-07). The authors are grateful to the staff from the 320 kV ECR HCIs platform at IMP (Lanzhou) and the staff of the Public Center and Nanobionics for their technical supports. We also thank Peng Lv, a joint-PhD student of Lanzhou University and Stockholm University, for supporting measuring of the $B^{[4]}$ content in NBS1-2 glasses used in this paper.

## ORCID

*Mengli Sun* https://orcid.org/0000-0001-5502-9212
*Sandro Jahn* https://orcid.org/0000-0002-2137-8833
*Haibo Peng* https://orcid.org/0000-0001-9117-0854
*Piotr M. Kowalski* https://orcid.org/0000-0001-6604-3458

## REFERENCES

1. Stoch P, Stoch A. Structure and properties of cs containing borosilicate glasses studied by molecular dynamics simulations. J Non Cryst Solids. 2015;411:106–14.
2. Webb S. Silicate melts: relaxation, rheology, and the glass transition. Rev Geophys. 1997;35(2):191–218.
3. Manaktala HK. An assessment of borosilicate glass as a high-level waste form. San Antonio, TX: Nuclear Regulatory Commission; 1992. CNWRA:92–017.
4. Ren M, Deng L, Du J. Surface structures of sodium borosilicate glasses from molecular dynamics simulations. J Am Ceram Soc. 2017;100(6):2516–24.
5. Deng L, Du J. Effects of system size and cooling rate on the structure and properties of sodium borosilicate glasses from molecular dynamics simulations. J Chem Phys. 2018;148(2):024504.
6. Kurkjian CR, Prindle WR. Perspectives on the history of glass composition. J Am Ceram Soc. 1998;81:795–813.
7. Wang M, Krishnan NA, Wang B, Smedskjaer MM, Mauro JC, Bauchy M. A new transferable interatomic potential for molecular dynamics simulations of borosilicate glasses. J Non Cryst Solids. 2018;498:294–304.
8. Jewell JM, Spess MS, Shelby JE. Effect of water concentration on the properties of commercial soda-lime-silica glasses. J Am Ceram Soc. 1990;73:132–5.

9. Bowles DE, Tompkins SS. Prediction of coefficients of thermal expansion for unidirectional composites. J Compos Mater. 1989;23:370–88.
10. Taurino R, Lancellotti I, Barbieri L, Leonelli C. Glass ceramic foams from borosilicate glass waste. Int J Appl Glass Sci. 2014;5(2):136–45.
11. Khemthong S, Hansen N, Bower M. Optimization and performance of space station freedom solar cells. Space photovoltaic Res Tech, 1989. 1991;400–9.
12. Sobolev IA, Dmitriev SA, Lifanov FA, Kobelev AP, Stefanovsky SV. Vitrification processes for low, intermediate radioactive and mixed wastes. Glass Technol. 2005;46(1):28–35.
13. Goel A, McCloy JS, Pokorny R, Kruger AA. Challenges with vitrification of Hanford high-level waste (hlw) to borosilicate glass an overview. J Non Cryst Solids X. 2019;4:100033.
14. Lutze W, Ewing RC. Radioactive waste forms for the future. Vol. 21. North-Holland: Elsevier Science Publishers B.V.; 2019.
15. Banerjee D, Sudarsan VK, Joseph A, Mishra R, Singh I, Wattal PK, et al. Role of tio2 on the physicochemical properties of cesium borosilicate glasses. J Am Ceram Soc. 2010;93(10):3252–8.
16. Peuget S, Cachia J-N, Jégou C, Deschanels X, Roudil D, Broudic V, et al. Irradiation stability of r7t7-type borosilicate glass. J Nucl Mater. 2006;354(1):1–13.
17. Weber WJ. Radiation and thermal ageing of nuclear waste glass. Procedia Mater Sci. 2014;7:237–46.
18. Peng H, Sun M, Yang K, Chen H, Yang D, Yuan W, et al. Effect of irradiation on hardness of borosilicate glass. J Non Cryst Solids. 2016;443:143–7.
19. Guan M, Zhang XY, Yang KJ, Wang TT, Liu FF, Sun ML, et al. Difference in radiation effects of sodium borosilicate glass and vitreous silica with ions. J Non Cryst Solids. 2019;518:118–22.
20. Peng HB, Sun ML, Du X, Yuan W, Yang D, Chen L, et al. Variation of hardness and modulus of borosilicate glass irradiated with kr ions. Nucl Instrum Methods Phys Res B. 2017;406:561–5.
21. Sun ML, Peng HB, Duan BH, Liu FF, Du X, Yuan W, et al. Comparison of hardness variation of ion irradiated borosilicate glasses with different projected ranges. Nucl Instrum Methods Phys Res B. 2018;419:8–13.
22. Wang T, Zhang X, Sun M, Du X, Guan M, Peng H, et al. irradiation effects in borosilicate glass studied by EPR and UV-VIS spectroscopies. Nucl Instrum Methods Phys Res B. 2020;464:106–10.
23. Jahn S, Kowalski PM. Theoretical approaches to structure and spectroscopy of earth materials. Rev Mineral Geochem. 2014;78(1):691–743.
24. Delaye JM, Ghaleb D. Combining two types of molecular dynamics for rapid computation of high-energy displacement cascades. I. Description of the method. Phys Rev B. 2005;71(22):224203.
25. Delaye J, Louis-Achille V, Ghaleb D. Modeling oxide glasses with Born-Huggins potentials: effect of composition on structural changes. J Non Cryst Solids. 1997;210(2):232–42.
26. Kieu LH, Delaye JM, Stolz C. Modeling the effect of composition and thermal quenching on the fracture behavior of borosilicate glass. J Non Cryst Solids. 2012;358(23):3268–79.
27. Chroneos A, Rushton M, Jiang C, Tsoukalas L. Nuclear waste-form materials: atomistic simulation case studies. J Nucl Mater. 2013;441(1):29–39.
28. Kieu LH, Kilymis D, Delaye JM, Peuget S. Discussion on the structural origins of the fracture toughness and hardness changes in rapidly quenched borosilicate glasses: a molecular dynamics study. Procedia Mater Sci. 2014;7:262–71.
29. Kilymis DA, Delaye JM, Ispas S. Nanoindentation of the pristine and irradiated forms of a sodium borosilicate glass: insights from molecular dynamics simulations. J Chem Phys. 2016;145(4):044505.
30. Yuan W, Peng H, Sun M, Du X, Lv P, Zhao Y, et al. Structural origin of hardness decrease in irradiated sodium borosilicate glass. J Chem Phys. 2017;147(23):234502.
31. Yuan W, Peng H-B, Du X, Lv P, Sun M-L, Chen L, et al. Origin of molecular oxygen formation in irradiated borosilicate glasses studied by molecular dynamics simulation. Int J Appl Glass Sci. 2018;9(3):344–51.
32. Zhao Y, Zhang X, Yuan W, Liu F, Sun M, Peng H, et al. Composition effects on mechanical properties of pristine sodium borosilicate glass. Int J Appl Glass Sci. 2019;10(3):363–70.
33. Kowalski PM, Ji Y, Li Y, Arinicheva Y, Beridze G, Neumeier S, et al. Simulation of ceramic materials relevant for nuclear waste management: Case of $La_{1-x}Eu_xPO_4$ solid solution. Nucl Instrum Methods Phys Res B. 2017;393:68–72.
34. Ji Y, Kowalski PM, Neumeier S, Deissmann G, Kulriya PK, Gale JD. Atomistic modeling and experimental studies of radiation damage in monazite-type lapo4 ceramics. Nucl Instrum Methods Phys Res B. 2017;393:54–8.
35. Chen L, Zhang D, Lv P, Zhang J, Du X, Yuan W, et al. Evolutions of molecular oxygen formation and sodium migration in Xe ion irradiated borosilicate glasses. J Non Cryst Solids. 2016;448:6–10.
36. Smedskjaer MM, Mauro JC, Youngman RE, Hogue CL, Potuzak M, Yue Y. Topological principles of borosilicate glass chemistry. J Phys Chem B. 2011;115(44):12930–46.
37. Plimpton S. Fast parallel algorithms for short-range molecular dynamics. J Comput Phys. 1995;117(1):1–19.
38. Gale JD, Rohl AL. The general utility lattice program (gulp). Mol Simul. 2003;29(5):291–341.
39. Guillot B, Sator N. A computer simulation study of natural silicate melts. Part I: low pressure properties. Geochim Cosmochim Acta. 2007;71:1249–65.
40. Kieu LH, Delaye JM, Cormier L, Stolz C. Development of empirical potentials for sodium borosilicate glass systems. J Non Cryst Solids. 2011;357:3313–21.
41. den Toonder JMJ, van Dommelen JAW, Baaijens FPT. The relation between single crystal elasticity and the effective elastic behaviour of polycrystalline materials: theory, measurement and computation. Modell Simul Mater Sci Eng. 1999;7(6):909–28.
42. Chen XQ, Niu H, Li D, Li Y. Modeling hardness of polycrystalline materials and bulk metallic glasses. Intermetallics. 2011;19(9):1275–81.
43. Chartier A, Meis C, Crocombette JP, Weber WJ, Corrales LR. Molecular dynamic simulation of disorder induced amorphization in pyrochlore. Phys Rev Lett. 2005;94:025505.
44. Crocombette JP, Chartier A. Molecular dynamics studies of radiation induced phase transitions in $La_2Zr_2O_7$ pyrochlore. Nucl Instrum Meth B. 2007;255(1):158–65.
45. Ji Y. Atomistic modeling of nuclear waste materials: cases of ceramic waste forms and nuclear graphite. Dissertation. Rheinisch-Westfalische Technische Hochschule Aachen; Aachen. 2018.
46. Turcotte RP, Wald JW. Devitrification behavior in a zinc borosilicate nuclear waste glass, IAEA Reports, Vol. 9, Report Number: PNL--2247, Reference Number 9412150. Richland, WA: Battelle Pacific Northwest Labs; 1978.
47. Smedskjaer MM, Mauro JC, Yue Y. Cation diffusivity and the mixed network former effect in borosilicate glasses. J Phys Chem B. 2015;119(23):7106–15.

48. Yun Y, Bray P. Nuclear magnetic resonance studies of the glasses in the system $Na_2O$-$B_2O_3$-$SiO_2$. J Non Cryst Solids. 1978;27(3):363–80.
49. Barlet M, Kerrache A, Delaye JM, Rountree CL. $SiO_2$-$Na_2O$-$B_2O_3$ density: a comparison of experiments, simulations, and theory. J Non Cryst Solids. 2013;382:32–44.
50. Feil D, Feller S. The density of sodium borosilicate glasses related to atomic arrangements. J Non Cryst Solids. 1990;119(1):103–11.
51. Budhwani K, Feller S. A density model for the lithium, sodium and potassium borosilicate glass systems. Phys Chem Glasses. 1995;36(4):183–90.
52. Inoue H, Masuno A, Watanabe Y, Suzuki K, Iseda T. Direct calculation of the physical properties of sodium borosilicate glass from its chemical composition using the concept of structural units. J Am Ceram Soc. 2012;95(1):211–6.
53. Michel F, Cormier L, Lombard P, Beuneu B, Galoisy L, Calas G. Mechanisms of boron coordination change between borosilicate glasses and melts. J Non Cryst Solids. 2013;379:169–76.
54. Weber WJ, Roberts FP. A review of radiation effects in solid nuclear waste forms. Nucl Technol. 1983;60:178–98.

**How to cite this article:** Sun M, Jahn S, Peng H, Zhang X, Wang T, Kowalski PM. Properties of irradiated sodium borosilicate glasses from experiment and atomistic simulations. *J Am Ceram Soc*. 2021;104:4479–4491. https://doi.org/10.1111/jace.17830